



Manganese dioxide nanoparticles/activated carbon composite as efficient UV and visible-light photocatalyst

Idrees Khan¹ · Muhammad Sadiq² · Ibrahim Khan³ · Khalid Saeed¹

Received: 29 August 2018 / Accepted: 19 December 2018 / Published online: 3 January 2019
© Springer-Verlag GmbH Germany, part of Springer Nature 2019

Abstract

Manganese dioxide nanoparticles/activated carbon (MnO₂/AC) composites and manganese dioxide nanoparticles (MnO₂ NPs) are prepared through chemical reduction method. Morphological study shows that MnO₂ NPs had cylindrical and spherical shape. The morphological study also revealed that MnO₂ NPs were well dispersed on AC while neat Mn NPs present both in dispersed and in agglomerated form. The FT-IR study confirms the synthesis of MnO₂ NPs. Zetasizer study presented that the Mn NPs had uniform size and below 100 nm in size and had zeta potential of – 20 mV, which represent its stability in the suspension form. The synthesized Mn/AC composite and Mn NPs were utilized as photocatalysts for the photodegradation of Congo red (CR) dye. The degradation study shows that MnO₂/AC composite degraded CR dye more efficiently than MnO₂ NPs under UV and normal light irradiation. The efficient degradation of dye by Mn/AC composite is due to the synergistic effect between dye adsorption on AC and rapid photodegradation by supported MnO₂ NPs. The results revealed that Mn/AC composite degraded about 98.53% of CR dye within 5 min while MnO₂ NPs degraded 66.57% of dye within the same irradiation time. The recycled catalyst also significantly degraded dye which verifies its sustainability. The effect of catalyst dosage and initial dye concentration was conducted. The degradation rate of dye was found drastically faster in tap water (in presence of catalyst), which might be due to the presence of various mineral ions in the tap water.

Keywords Manganese dioxide, nanoparticles · Activated carbon · Photodegradation · Congo red · Photocatalyst

Introduction

Organic dyes are common water pollutants frequently found in the effluents of various industries such as textile, leather, food cosmetics, and paper (Mohamed et al. 2016; Wu et al. 2016). The various synthetic organic dyes are the major water pollutants and make the environmental problems seriously due to their large-scale production, low biodegradability, high aromaticity, chemical stability, toxicity, and carcinogenic in nature (Velusamy and Lakshmi 2017;

Zhao et al. 2018a, b, c). These colored wastewater discharge even with a small quantity of dyes can lead to the development of color in the whole aquatic system which causes severe environmental problems (Shivaraju et al. 2017). The efficient removal of organic dyestuffs in industrial polluted water is a challenging hot issue in the field of environmental remediation and pollution control (Pan et al. 2018a, b). Various conventional physical, biological, and chemical methods were employed for dye removal such as adsorption, flocculation, electro-transformation, precipitation, ozonization, reverse osmosis, and ultrafiltration (Saeed et al. 2015; Huang et al. 2017). These conventional methods are difficult to handle, not economic, non-destructive, and only transfer the pollutant matter into sludge and give rise to a new type of pollution, which needs further treatment (Shivaraju et al. 2017; Sangami and Dharmaraj 2012). Each of these methods has their own disadvantages, i.e., microorganisms aerobically oxidize the dyes partially and result in the formation of volatile carcinogenic compounds (Padikkaparambil et al. 2013). Similarly, adsorption and membrane filtration techniques are relied on the

Responsible editor: Suresh Pillai

✉ Khalid Saeed
khalidkhalil2002@yahoo.com

¹ Department of Chemistry, Bacha Khan University, Charsadda, Khyber Pakhtunkhwa, Pakistan

² Department of Chemistry, University of Malakand, Chakdara, Dir (L), Khyber Pakhtunkhwa, Pakistan

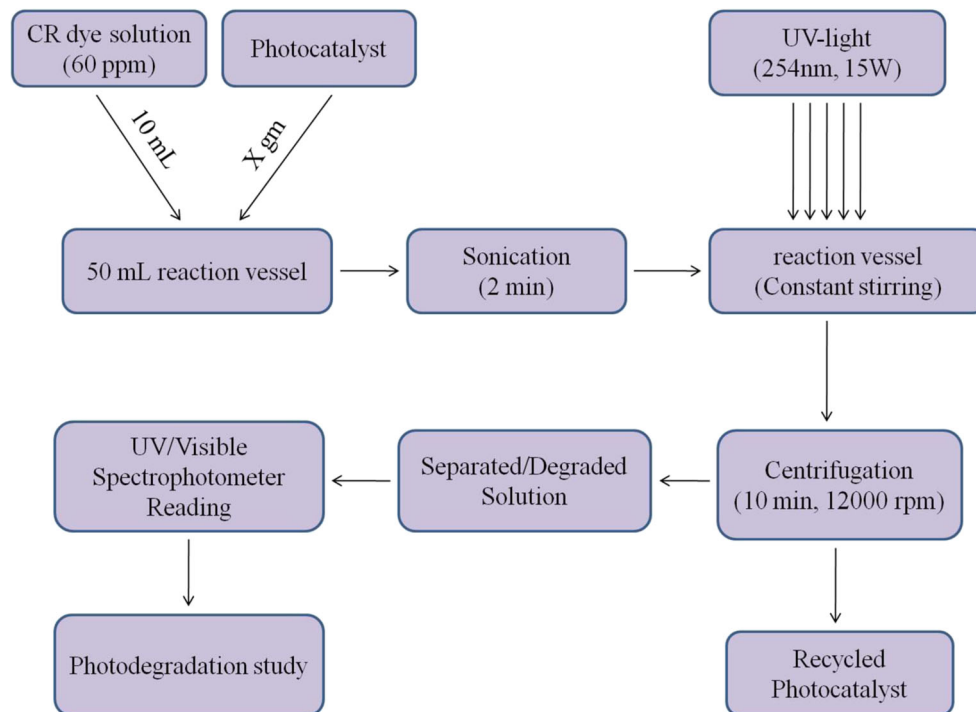
³ Department of Chemistry, King Fahd University of Petroleum and Minerals, Dhahran 31261, Saudi Arabia

production of secondary pollutants, and ecologically, these are not viable methods (Shivaraju et al. 2017). These methods require further treatment for solid wastes and regeneration of adsorbent which will increase cost of the process (Akpan and Hameed 2009). The development of efficient approach for elimination and degradation of harmful pollutants is of great significance and has become one of the most hot research fields (Pan et al. 2018a, b; Zhao et al. 2018a, b, c). Recently, semiconductor photocatalysis is an emerging and promising technology for waste effluent treatment because it is efficient, economical, and environmental friendly and has the capability to decolorize and degrade the dye molecules into simple and non-toxic inorganic species such as carbon dioxide and water (Mamba et al. 2015; Wu et al. 2010; Zhao et al. 2018a, b, c). This technology has the capability of degrading a wide range of organic compounds and converts these pollutants into harmless substances directly in waste water (Zhang and Zeng 2010; Wang et al. 2007). In this technology, metal oxide nanoparticles (NPs) are explored as photocatalysts for decomposition of organic pollutants (Zhang and Zeng 2010). Metals NPs show good photocatalytic activity due to its chemical stability, uniform pore size, high surface area, and low photo-corrosion and hence enhance photodegradation rate and degradation efficiency (Pouretedal and Kiyani 2014). Nanoparticles tend to form strong agglomerates, but in most applications, NPs are required to be in well-dispersed form, which requires extremely high specific energy in order to overcome the

adhesive forces (Saeed et al. 2018). In photocatalysis, the metal NPs in suspended form show several difficulties such as aggregation in bulk solution and its separation from solution after reaction, small amount of absorbed photons in the visible light region, and high recombination of the photogenerated electron–hole pairs on the photocatalyst surface (Soltani and Haghighat 2016; Su et al. 2018). These deficiencies have been overcome by various approaches such as doping and co-doping (Hamukwaya et al. 2019), coupling with narrow band gap semiconductors (Zhang et al. 2017a, b) dispersing NPs in the polymer matrix (Saeed et al. 2018), dispersing on support materials (Zada et al. 2017) etc. Among these methods, synthesizing NPs on support materials is a simple way to retard NP agglomeration. Various support materials were reported for the NP synthesis such as multi-walled carbon nanotubes (Zada et al. 2017; Koo et al. 2014), TiO₂ (Rout et al. 2015), diatomite (mainly composed of SiO₂) (Soltani and Haghighat 2016) etc.

In the present study, cost-effective activated carbon (AC) was prepared from peanut shell and utilized as a support materials for synthesis of NPs. Various carbon materials and their composites are reported for various applications such as carbon black, carbon fibers, carbon nanotubes, flexible graphite, graphene nanosheets, graphene oxide, and reduced graphene oxide for EMI shielding (Wang et al. 2018) polycarbonate/carbon nanotubes selective oil adsorption from water (Li et al. 2018), magnetic carbon nano adsorbents for chromium removal (Huang

Fig. 1 A general scheme of working method



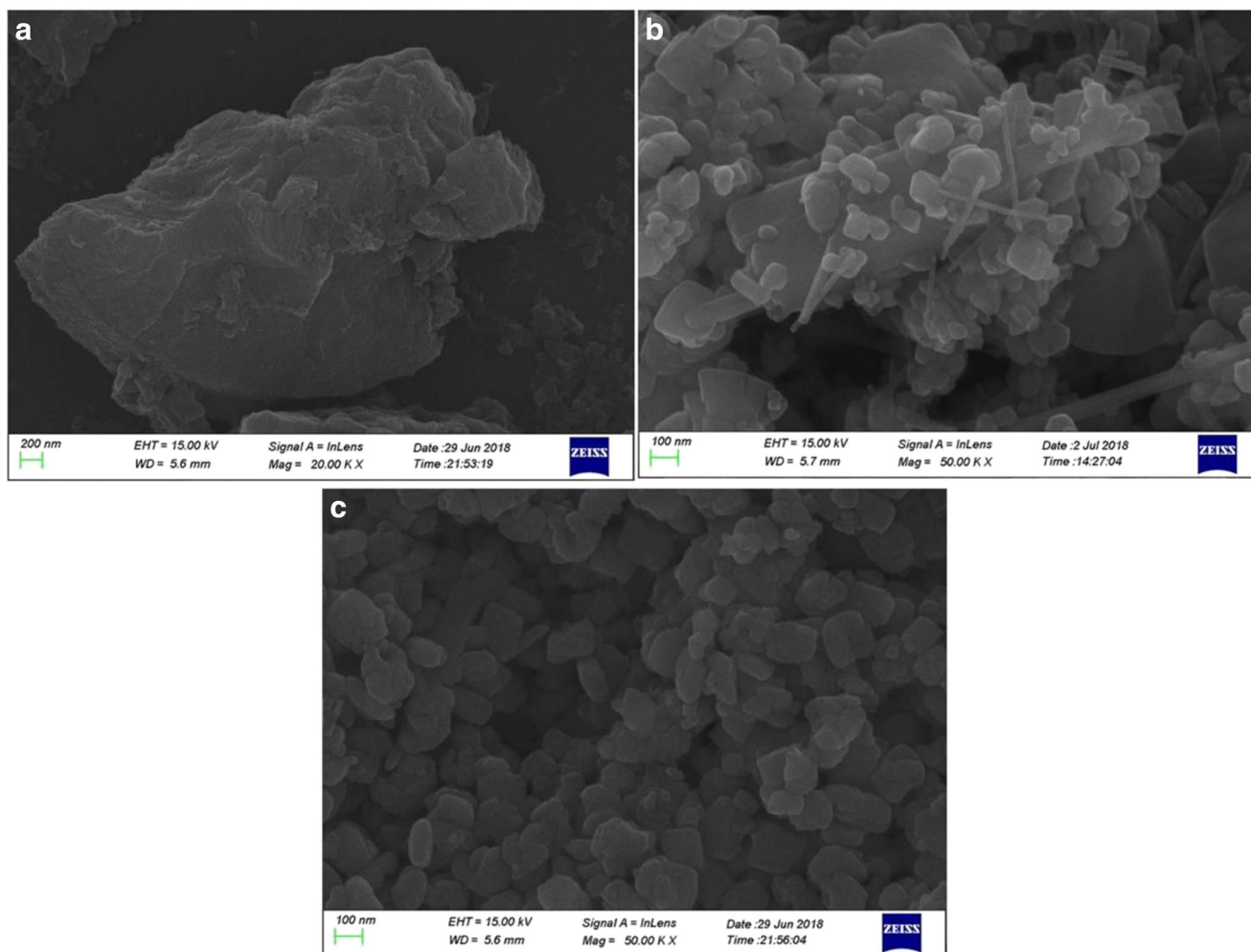


Fig. 2 SEM images of **a** AC, **b** MnO_2/AC composite, and **c** MnO_2 NPs

et al. 2018), nano- TiNb_2O_7 /carbon nanotube composite for enhanced lithium-ion storage (Lin et al. 2018), reduced graphene oxide-cuprous oxide nanocomposites for long-term antibacterial activities (Yang et al. 2019), iron-nitrogen-carbon nanoparticle modified porous graphene (Fe-N-C/PGR) for oxygen reduction reaction (Zhang et al. 2018). AC are highly microporous carbon having high surface area and high porosity, low cost, good resistance to extreme condition commercially the most common adsorbents and often serve as catalysts and catalyst supports (Ioannidou and Zabaniotou 2007; Gong et al. 2018). MnO_2/AC composite and neat MnO_2 NPs were prepared through simple chemical reduction method using NaOH as a reducing agent and were characterized by various instrumental techniques like atomic force microscopy (AFM), scanning electron microscopy (SEM), energy dispersive X-ray (EDX), and zeta potential. Manganese oxides in micro and nanosize have wide range of applications in the field of catalysis, rechargeable batteries, ion sieves, chemical sensing devices, field-emission devices, magnetic devices, hydrogen storage media, and microelectronics

(Dang et al. 2015) MnO_2/AC composite and neat MnO_2 NPs were used as photocatalysts for the photodegradation of CR dye. CR dye is a well-known azo dye that is highly toxic and even carcinogenic to human and animals. CR dye is not readily degradable and cause severe environmental problems when discharged from textile dyeing industries (Liu et al. 2013). Various studies have been performed for the photodegradation of CR but these studies showed long irradiation time (30–180 min) to obtain maximum degradation efficiency (Erdemoglu et al. 2008; Melghit and Al-Rabaniah 2006; Zhua et al. 2009). Therefore, it is needed to prepare a new photocatalyst based on AC and Mn NPs to degrade CR dye in a minimum time and to identify optimum parameters that can allow maximum effectiveness in photodegradation of CR dye. In the present study, an attempt is made to achieve the efficient and fast photodegradation of CR dye by using MnO_2/AC and MnO_2 NPs as photocatalysts for CR degradation. The effect of several parameters such as irradiation time, catalyst amount, initial dye concentration, light source, recycled catalyst activity, and effect of tap water was evaluated.

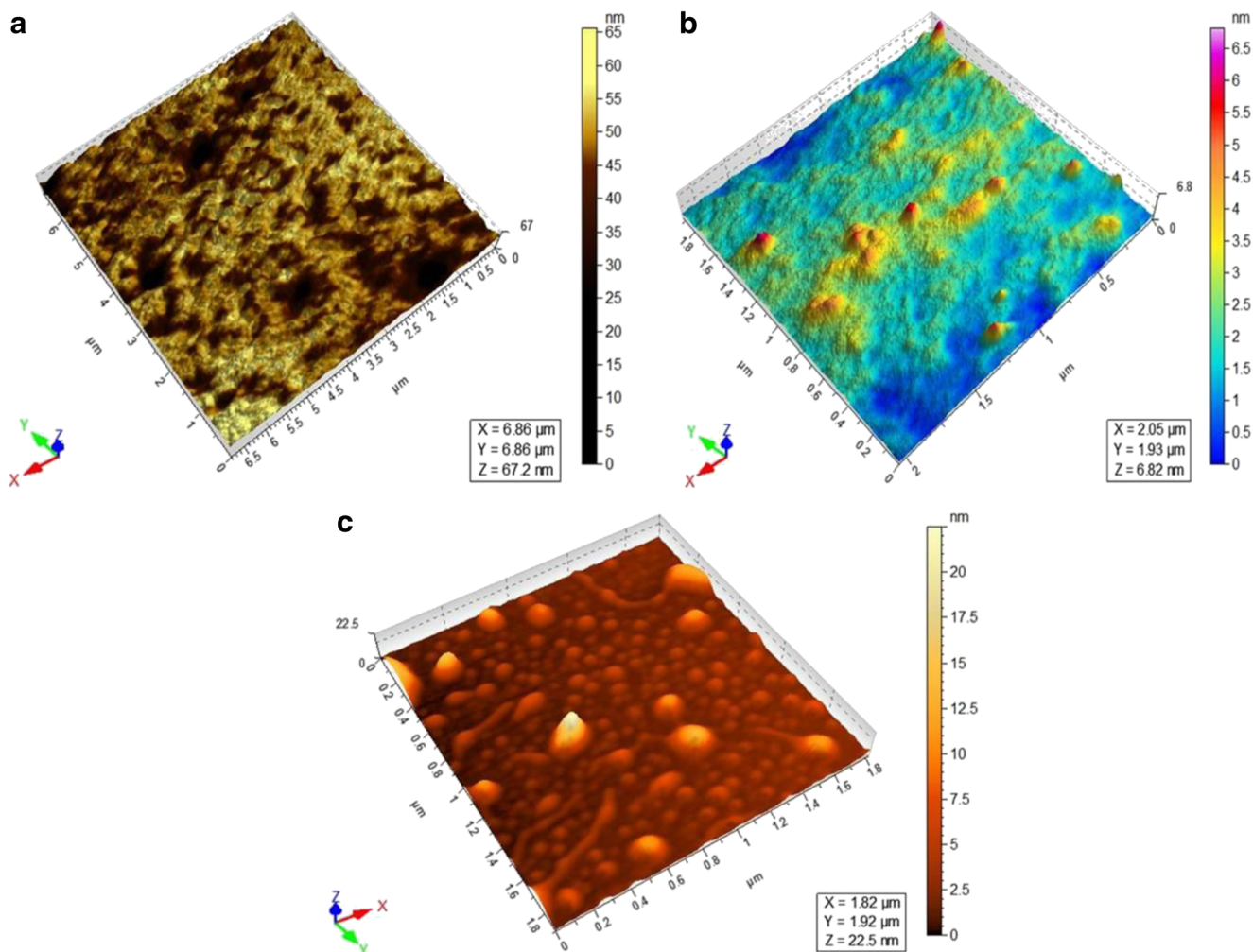


Fig. 3 AFM 3D images of a AC, b MnO₂/AC composite, and c MnO₂ NPs

Experimental works

Materials

Milled peanut (*Arachis hypogaea*) shell was purchased from the local market. Phosphoric acid, sodium hydroxide, and CR dye were supplied by Sigma-Aldrich and were used as received. Hydrogen, oxygen, and nitrogen gases were supplied by BOC Pakistan and were further purified with appropriate filter.

Synthesis of activated carbon

The raw peanut shells (200 g) were purified and oven-dried at 105 °C for 12 h. After complete drying, the sample was soaked in H₃PO₄ (15%) for 24 h in the 1:1 (g of peanut shell/mL of acid solution). The soaked sample is then washed in a modified soxhlet apparatus until neutral pH was reached. The sample was then carbonized in a tube furnace (reactor: quartz, diameter of 4 cm and length 50 cm) at 380 °C for 1 h in

an inert atmosphere. The sample was activated in H₂O₂ via sonication for 30 min. Finally, the AC was washed in a modified soxhlet apparatus, dried, and meshed (US standard sieves). The thermal treatment of sample was performed at 580 °C with a rate of 5 °C/min and held for 2 h under N₂, in order to tune the surface of AC for desired functional group. After activation and high temperature treatment, the weight of the sample was 16.3 g, which show 91.8% weight loss.

Synthesis of Mn/AC composite and Mn NPs

In a volumetric flask, 100 mL MnCl₄·2H₂O (0.5 M) and 1 g of AC were taken, sonicated for 1 h for complete dispersing AC in solution and stirred occasionally. NaOH solution (2 M) was added drop wise to the mixture until the pH reached to 9 under constant stirring. The reaction mixture then refluxed at 100 °C for 2 h with constant stirring, and as result, the precursor metal salt reduced into corresponding NPs on the AC surface. The solution mixture is then cooled to room temperature, filtered, and washed many times with distilled water in order to

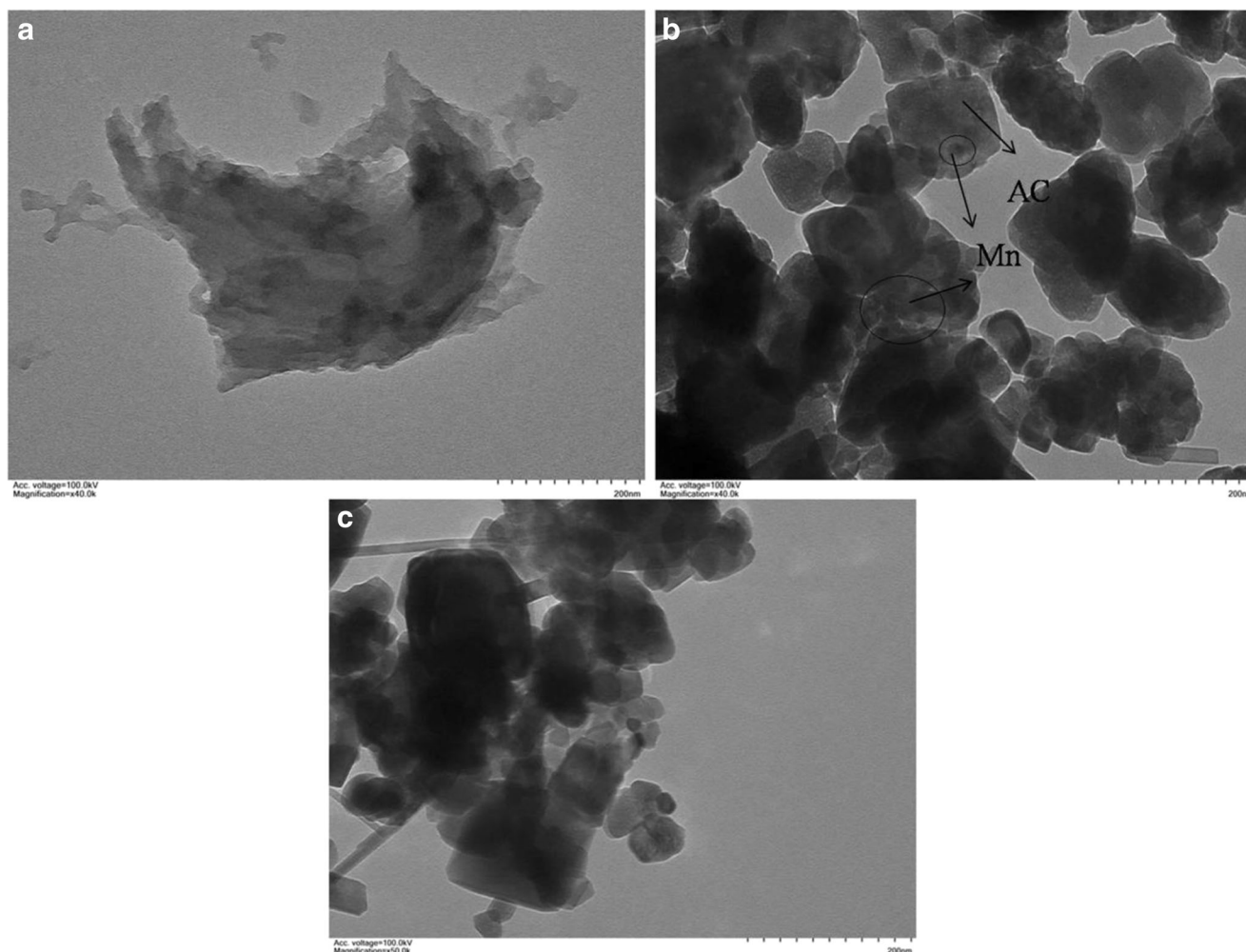


Fig. 4 TEM images of **a** AC, **b** MnO₂/AC composite, and **c** MnO₂ NPs

remove the unwanted chemicals. The obtained MnO₂/AC (2.4:1) composite was then completely dried at 90 °C for 10 h in an oven and stored. The same procedure is followed for the synthesis of neat MnO₂ NPs except the addition of AC.

Photodegradation of CR dye

The photocatalytic activity of the MnO₂/AC composite and MnO₂ NPs was tested for the photodegradation of CR dye as a function of several parameters. In a typical reaction, 10-mL CR dye solution (60 ppm) was taken in a beaker (50 mL) and a known quantity of photocatalyst was added to it. The mixture was sonicated for 2 min and irradiated under UV-light (254 nm, 15 W) or visible light for specific time. After completion of the reaction time, the catalyst was separated through centrifugation (10,000 rpm/min). The general scheme of working method is shown in Fig. 1. The photodegradation study was conducted by UV-Visible spectrophotometer. The %degradation of CR dye was calculated by using the following formula:

$$\text{Degradation Rate (\%)} = \frac{C_o - C}{C_o} \times 100$$

$$\text{Degradation Rate (\%)} = \frac{A_o - A}{A_o} \times 100$$

where C_o is the initial dye concentration, C is the dye concentration after UV irradiation, A_o shows the initial absorbance, and A shows the dye absorbance after UV irradiation.

Characterizations

The morphological study was performed by SEM (JEOL, JSM-5910, Company Japan) and AFM (5500, Agilent, Santa Clara, USA). The elemental composition study was performed by EDX spectrometer (Inea 200, UK, company oxford). The particle size, PDI, and zeta potential were determined by Zetasizer (ZS-90 Malvern instruments, Malvern, UK). The photodegradation study was monitored by UV/Visible spectrophotometer (Shimadzu 1800, Japan).

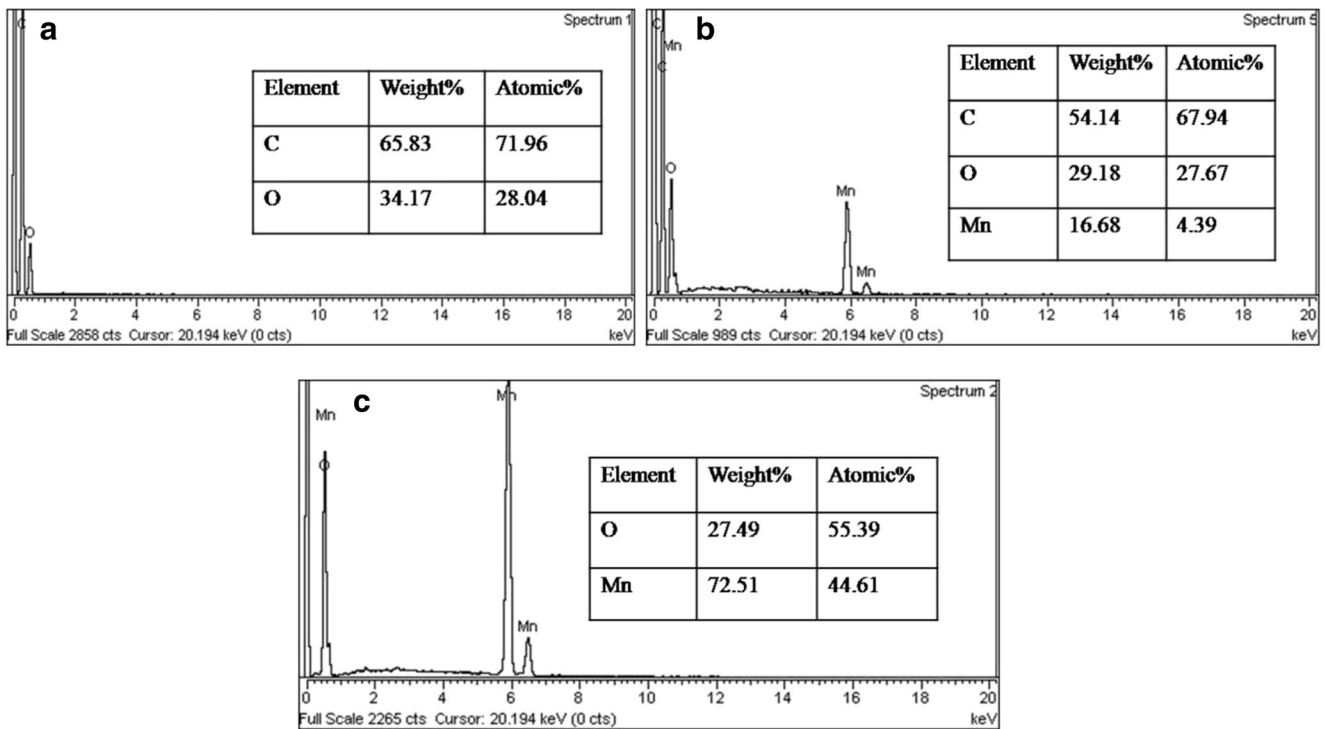


Fig. 5 EDX spectra and elemental compositions of **a** AC, **b** MnO₂/AC composite, and **c** MnO₂ NPs

Results and discussion

Morphological study

The morphological studies of catalysts/materials are very important for analyzing the size, shape, and surface, which is directly related to the catalytic activity. Figure 2a–c shows the SEM images of AC, MnO₂/AC composite, and MnO₂ NPs, respectively. Figure 2b shows that the NPs were well dispersed on the surface of AC. The micrographs also presented the presence of NPs inside the pores of AC. The neat MnO₂

NPs (Fig. 2c) were present both in dispersed and agglomerated form. Figure 2 shows the AFM 3D images of the AC, MnO₂/AC composite, and MnO₂ NPs. Figure 3a shows that

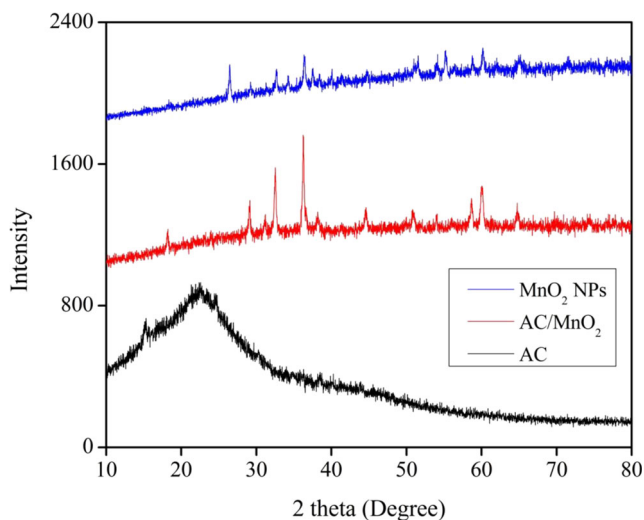


Fig. 6 XRD pattern of the AC, MnO₂/AC nanocomposite, and MnO₂ NPs

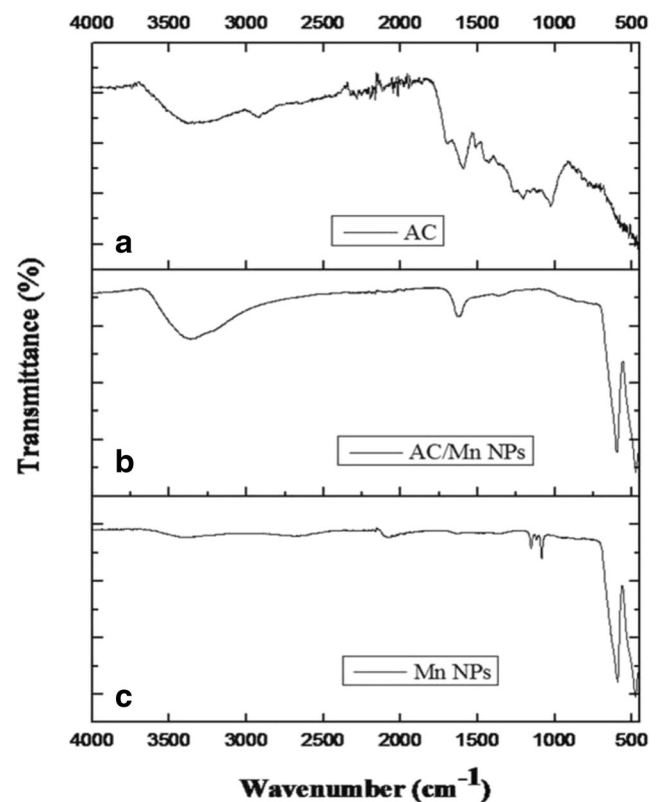


Fig. 7 FTIR spectra of **a** AC, **b** MnO₂/AC composite, and **c** MnO₂ NPs

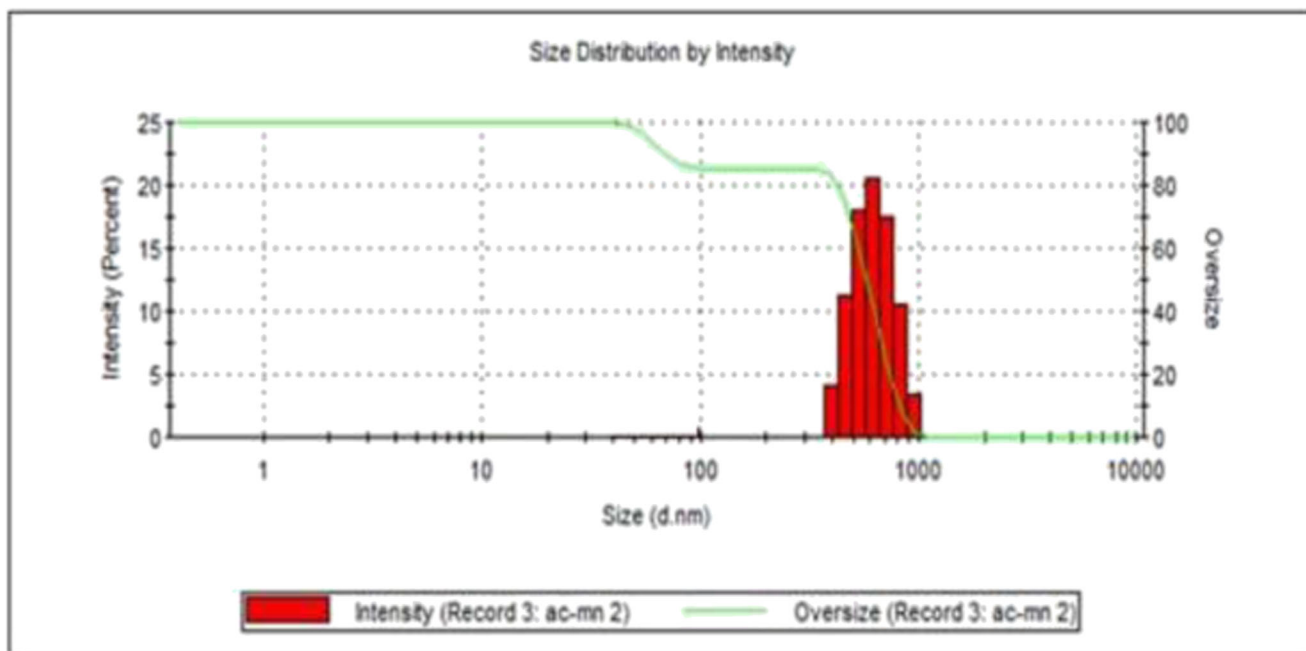


Fig. 8 Size and size distribution plot of MnO₂ NPs (average size 532 nm, PDI 0.34)

AC had uniform surface. The AFM image of MnO₂/AC composite (Fig. 2b) shows that the MnO₂ NPs are well dispersed on the surface of AC while the MnO₂ NPs (Fig. 3c) are present both in dispersed and agglomerated (some portion). The size of MnO₂ NPs measured from the 3D AFM images is mostly below 100 nm. The morphological study also illustrated that the NPs are spherical in shape.

The deep investigation about the phase, size, and morphology has been carried out by using transmission electron microscopy (TEM). Figure 4a–c shows the TEM images of AC,

MnO₂/AC NPs, and MnO₂ NPs, respectively. The AC had a rough surface (4a) while in composite, the MnO₂ NPs are well deposited and dispersed on its AC surface (4b). Figure 4c shows that MnO₂ NPs have no uniform morphology and in agglomerated form.

Elemental composition study

Elemental composition study provides information about the particular material synthesis and its purity. Figure 5a–c shows

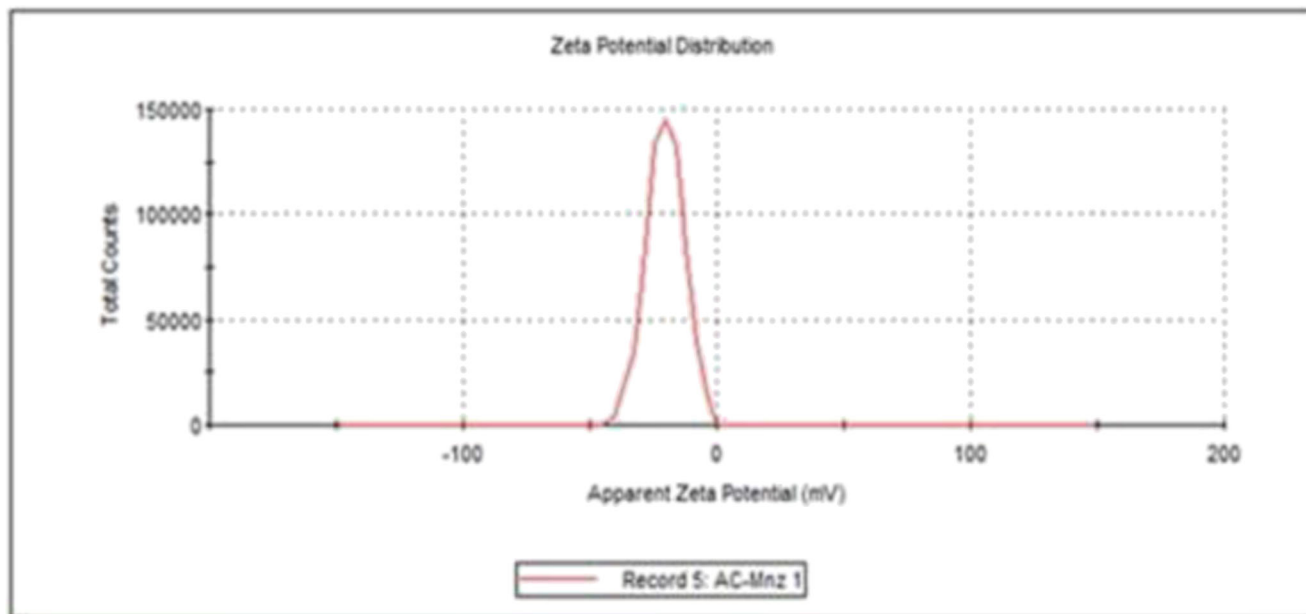


Fig. 9 Plot of total counts versus zeta potential (mV) of MnO₂ NPs

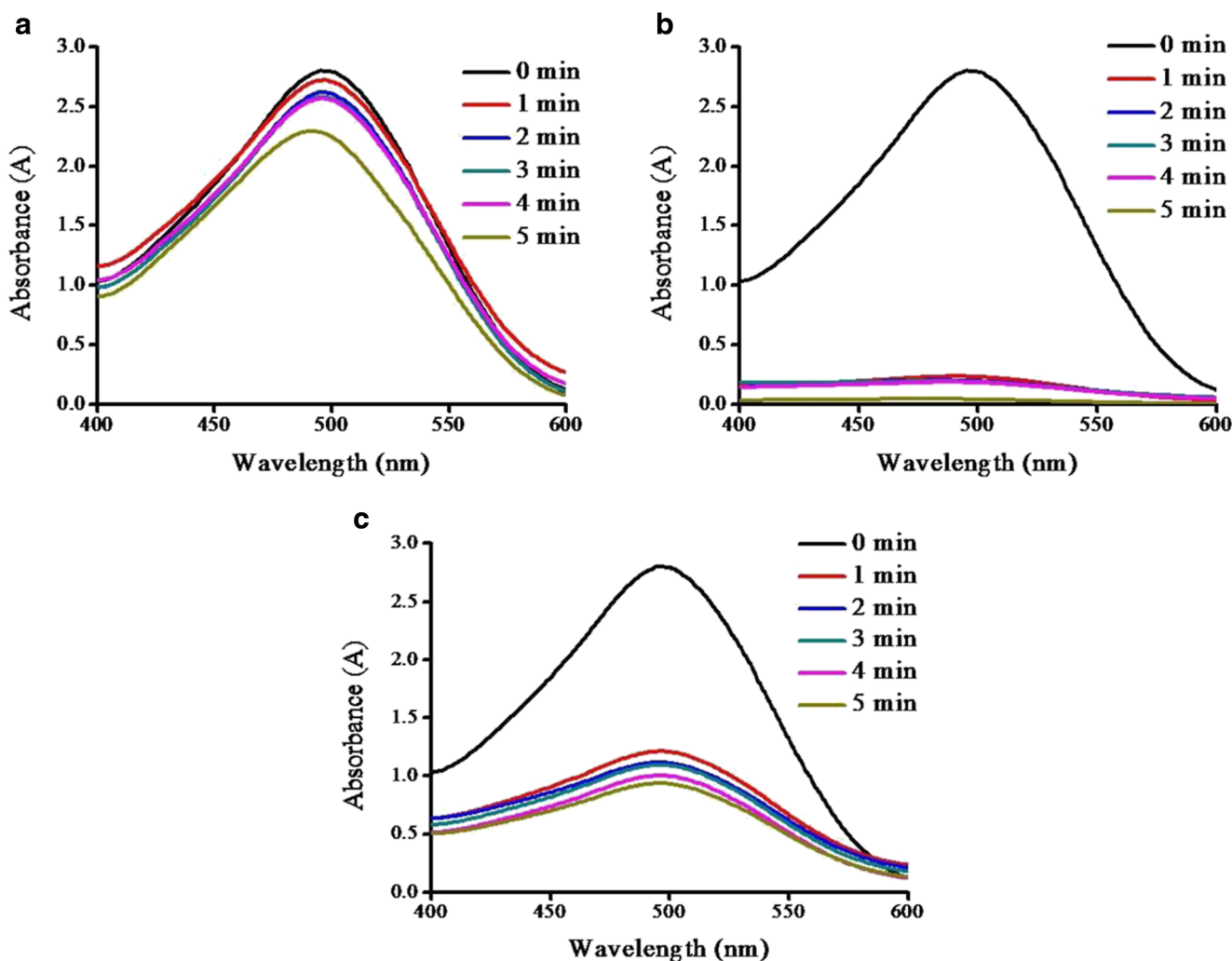


Fig. 10 UV-Vis spectra of CR dye before and after different UV-light irradiation times of a AC, b MnO₂/AC composite, c MnO₂ NPs

the EDX spectrum of AC, MnO₂/AC nanocomposite, and MnO₂ NPs, respectively. Figure 5a shows the peak for C and O while Fig. 5b contains the constituent elements C, O, and Mn which confirmed the formation of MnO₂ NPs on the surface of AC. Figure 5c shows Mn and O peak, which revealed the synthesis of oxide nanoparticles. Figure 5 also shows the % composition of the corresponding constituent elements.

XRD study

XRD study was carried out to examine the crystalline phase of manganese dioxide and its composite and also to check its impurity. Figure 6 shows the XRD pattern of the AC, MnO₂/AC nanocomposite, and MnO₂ NPs. The broad peak in AC observed around at 2θ = 24° correspond to the reflection of (002) plane is due to the amorphous structure of AC while the peak 2θ = 42° due to the reflection of (100) plane is attributed to graphite like structure (Sadiq et al. 2017). The peak appeared at 37.49° and 41.62°, which indicates the

formation of tetragonal MnO₂ which were indexed to (211) and (420) planes. The presences of other peaks indicate the polycrystalline nature of the MnO₂ nanoparticle (Ganeshan et al. 2017). The other respective peaks of MnO₂ are in good agreement with the reported literature (Feng et al. 2014).

FTIR study

FTIR spectroscopy is known for its high sensitivity, especially in the detection of inorganic and organic species. Figure 7a–c shows the FTIR spectra of AC, MnO₂/AC composite, and MnO₂ NPs. The peaks (Fig. 7a) that appeared at 2925 and 1615 cm⁻¹ were due to the stretching and bending vibration of C–H and NH groups, respectively. The peaks that appeared at 1249, 1045, 2377, and 1514 cm⁻¹ represent the C–C skeletal, C–N stretching, CO₂ asymmetric stretching, and N=O stretching vibration. Figure 7b shows the peak for both AC and Mn NPs and no new peaks were found, which conform that MnO₂ NPs are only deposited on the surface of AC without any chemical interactions. Figure 7c shows two absorption bands at

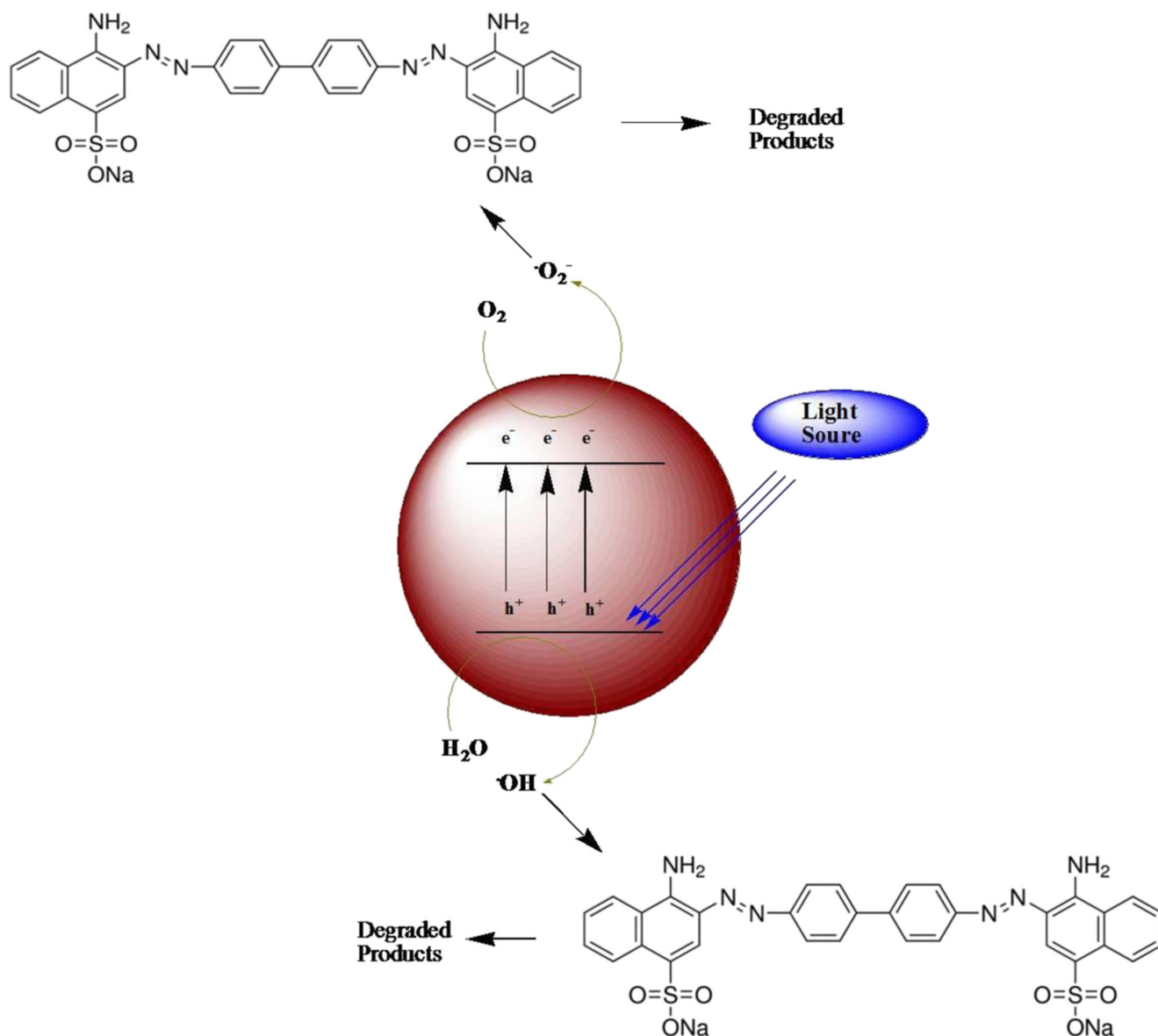


Fig. 11 General proposed mechanism for CR dye photodegradation

about 600 and 475 cm^{-1} that corresponded to the characteristic stretching vibration of O–Mn–O, which demonstrated the synthesis of the MnO_2 nanoparticles (Jaganyi et al. 2013).

Particle size and zeta potential

The particle size distribution is very important for finding out the regularity in the size of NPs and its zeta potential displays its stability. Figure 8 shows the size distribution plot of MnO_2 NPs, which represent that the average particle size was 532 nm which were quite larger than the size measured from SEM and AFM. It might be due to the swelling of particles in aqueous medium. The size measured from the DLS is actually the hydrodynamic size of particles so result of AFM and DLS usually shows

variation. The MnO_2 NPs have a polydispersity index (PDI) of 0.34 which reveals small variation in the particle size. The MnO_2 NPs seem to be very stable due to its -20.4 mV (Fig. 9), which show the zeta potential of the NPs, confirm that the MnO_2 NPs has high surface charge, and thus can be remained in suspended form in solution.

Photodegradation study

The photocatalytic activity of AC, MnO_2/AC nanocomposite, and MnO_2 NPs was evaluated by degrading CR dye under UV and normal light irradiation. Figure 10 shows the UV-Visible spectra of CR dye before and after UV-light irradiation in the presence of AC, MnO_2/AC nanocomposite, and MnO_2 NPs. The photodegradation of the dye was measured from its UV-

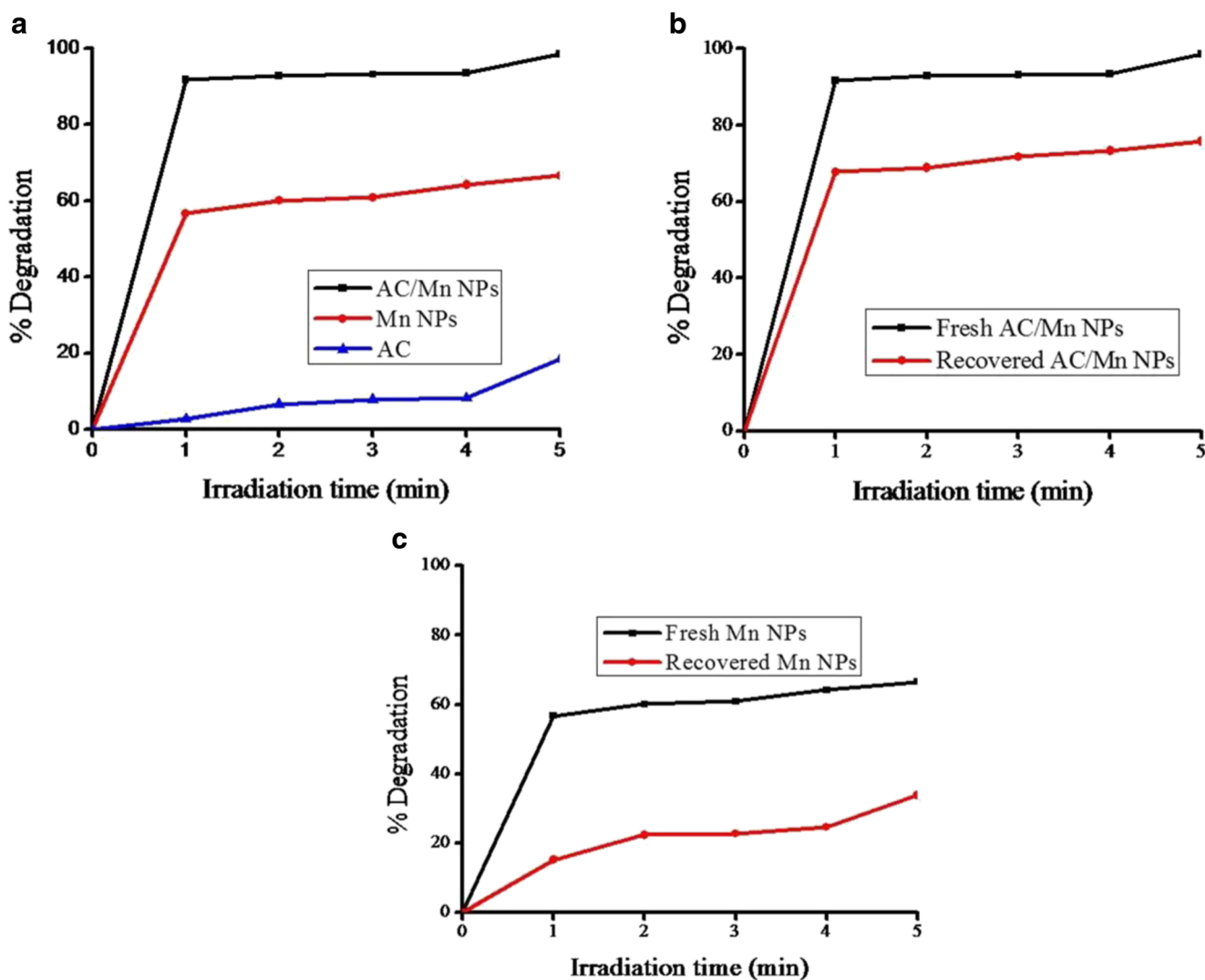


Fig. 12 Degradation comparison of CR dye photodegraded by **a** AC, MnO₂/AC composite and MnO₂ NPs, **b** fresh and recovered MnO₂/AC composite, **c** fresh and recovered MnO₂ NPs

Visible spectra which gave a maximum absorbance peak at 496 nm. The results show that the absorbance peak decreases with increasing irradiation time, which mean the rate of photodegradation increased. Figure 10a illustrates that AC is not effective as catalyst for the degradation of dye and found minute reduction in dye concentration, which might be the adsorption of CR dye rather than photodegradation. Figure 10b, c shows the degradation of CR in the presence of MnO₂/AC composite and MnO₂ NPs dye, which were significantly degraded by increasing the irradiation time. It was also found that the rate of photodegradation is much higher in the presence of MnO₂/AC NPs as compared to MnO₂ NPs, although the composite had less quantity of MnO₂ NPs. The high/faster degradation of dye might be due to the better dispersion (mean large surface area) of NPs on the surface of AC. Song et al. (2017) prepared carbon nanodots/WO₃ photocatalysts for photocatalytic degradation of Rhodamine

B and found that carbon nanodots/WO₃ possessed stronger photocatalytic activity than WO₃ and C-dots.

The photodegradation of dye is achieved when light falls upon MnO₂ NPs results in electron (e⁻) excitation from valence band to the conduction band, creating positively charged hole (h⁺) in the valence band. In case of neat Mn NPs that mostly present in agglomerated form, a greater portion of created electron-hole pairs recombine and thus show less photocatalytic activity. The composite (MnO₂/AC) shows enhanced activity because of having synergistic effect in reducing the recombining deficiency of created charges, high surface area of MnO₂ NPs on AC surface, and rapid dye adsorption by AC followed by its drastic degradation by supported MnO₂ NPs. The hole reacts with H₂O molecules and produces hydroxyl radicals (OH) while the e⁻ present in the conduction band reacts with oxygen molecule and produces superoxide anion radical (O₂⁻). These generated radicals are highly

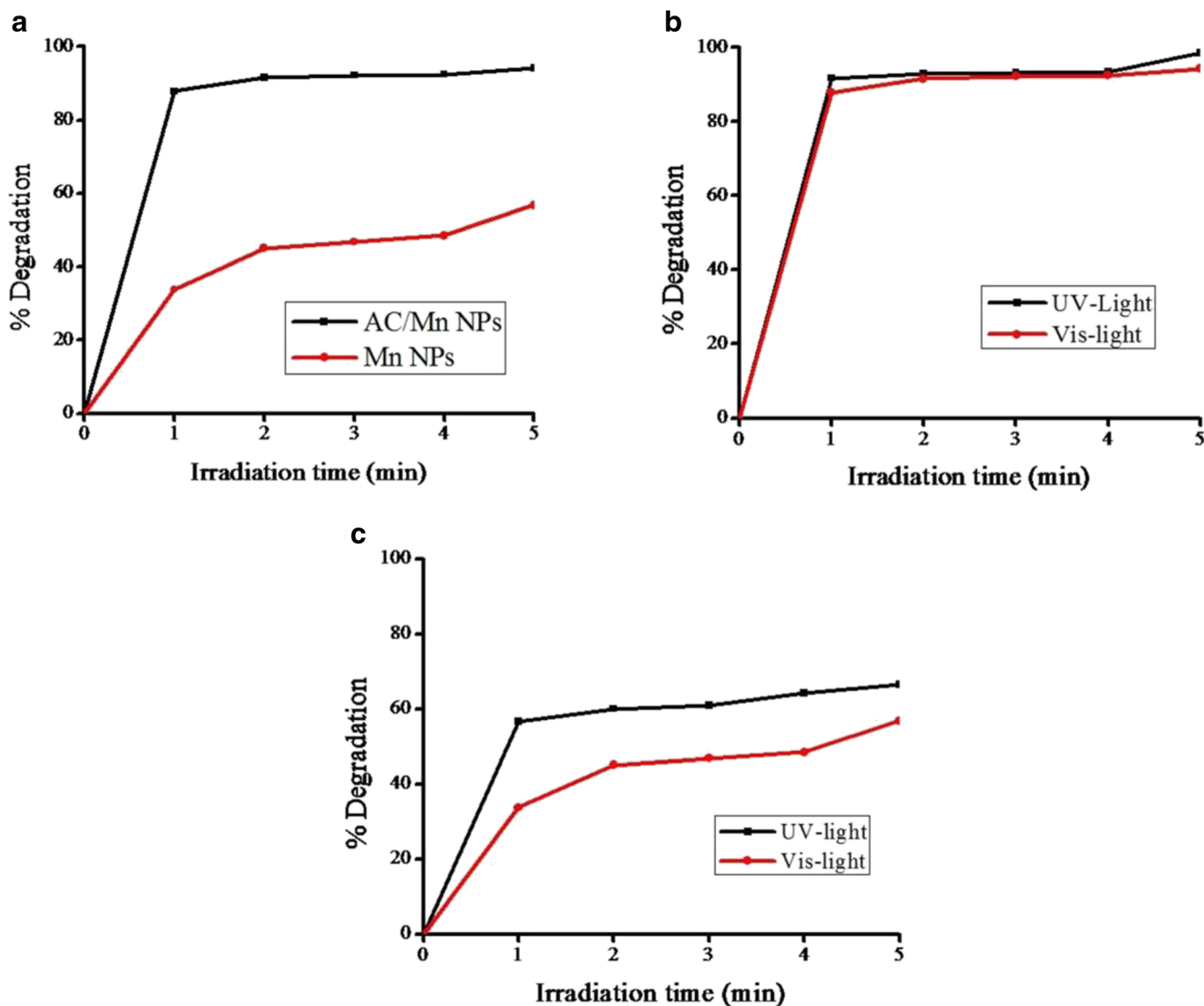
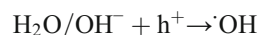
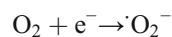
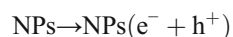


Fig. 13 Degradation comparison of CR dye degraded by **a** MnO₂/AC composite and MnO₂ NPs under visible light, **b** Mn/AC composite under UV and visible light, and **c** MnO₂ NPs under UV and visible light

reactive and degraded dye molecules into simpler species. The possible reaction steps in this mechanism are summarized in the following equations (Zada et al. 2017).



The possible reaction mechanism can easily be understood from the Fig. 11.

Figure 12a represents the % degradation of CR dye in the presence of AC, MnO₂/AC composite, and MnO₂ NPs. The results revealed that within the maximum irradiation

time of 5 min, the AC removed 18.42% while Mn NPs degraded 56.67 and 66.57% dye within 1 and 5 min, respectively. The MnO₂/AC composite degraded about 91.67% dye within 1 min which increased to 98.53% by increasing irradiation time to 5 min. The overall results are shown in Fig. 12a.

The effect of recycled catalyst was also studied by using the recycled MnO₂/AC composite and MnO₂ NPs under the same experimental conditions. The used catalysts were washed with distilled water via sonication in order to remove any adsorbed dye molecule and then oven dried at 100 °C. Figure 12b shows the % degradation comparison of CR dye in the presence of fresh and recycled MnO₂/AC composite. The results revealed that the recycled catalyst also show good catalytic activity but show less activity as compared to the fresh photocatalyst. The fresh MnO₂/AC composite degraded 98.53% dye while the recycled 75.78% dye within the same

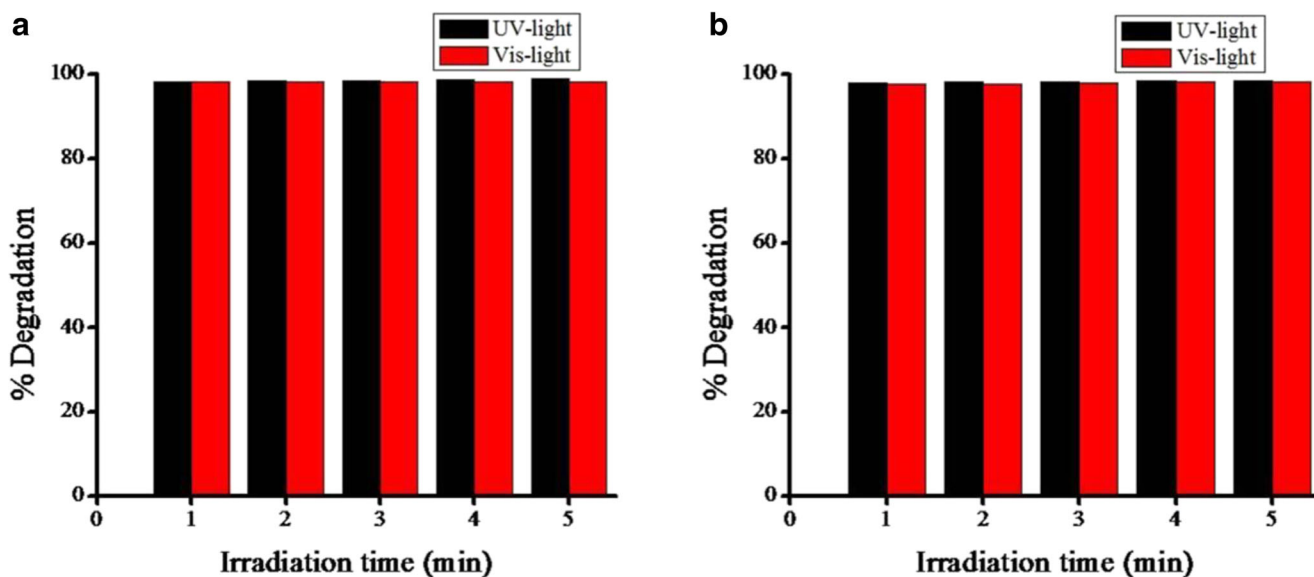


Fig. 14 Comparison of degradation rate of CR dye under UV and visible light photodegraded a MnO₂/AC composite and b MnO₂ NPs

irradiation time of 5 min. Similarly, the fresh MnO₂ NPs photocatalytically degraded 66.57% dye in 5 min while the recycled degraded 33.82% dye within the same irradiation time (Fig. 12c). Such decrease in the photocatalytic activity of the recycled catalysts might be the blockage of surface active sites due to the deposition of photo insensitive hydroxides (Zada et al. 2017).

Figure 13 represents the % degradation of CR dye degradation under visible light in the presence of MnO₂/AC composite and MnO₂ NPs. It was found that the MnO₂/AC composite was also very effective in the visible region and efficiently degraded dye under visible light irradiation while the MnO₂ NPs were less effective in the visible region. The MnO₂/AC composite degraded 94.21% dye within 5 min while the MnO₂ NPs degraded 56.78% dye within the same time under visible light. Figure 13b, c shows the comparison

of %degradation of CR dye under UV and visible light photodegraded by MnO₂/AC composite and MnO₂ NPs, respectively. The figure revealed that MnO₂/AC NPs are also significantly degraded the dye under the visible region and show almost the same activity as in the UV region while MnO₂ NPs are less effective in the visible region.

Effect of tap water

The effect of tap water on CR dye degradation was also studied by preparing the dye solution in tap water and then performed the reactions under the same experimental conditions. CR dye degraded very efficiently under both UV and visible light in a very short time. Figure 14a, b shows the comparison of % degradation of CR dye photodegraded by MnO₂/AC composite and MnO₂ NPs under UV and visible light. The graphs show that dyes were completely degraded in 1 min and need no further time. The results show that both the Mn/AC composite and Mn NPs photocatalysts degraded about 97–99% dye both under UV and visible light irradiation (1–5 min irradiation time). Such unpredicted enhancement in dye photodegradation might be due to the presence of various types of minerals ion in tap water.

Effect of catalyst dosage

Figure 15 shows the photodegradation of CR dye (UV-Visible spectra) in the presence of different dosage of MnO₂/AC (15a) composite and MnO₂ NPs (15b). Figure 15c shows the comparison of % degradation of CR dye in the presence of different amount of MnO₂/AC composite and MnO₂ NPs. It was found that the photodegradation of dye increased as the quantity of catalysts increased. The results also show that the

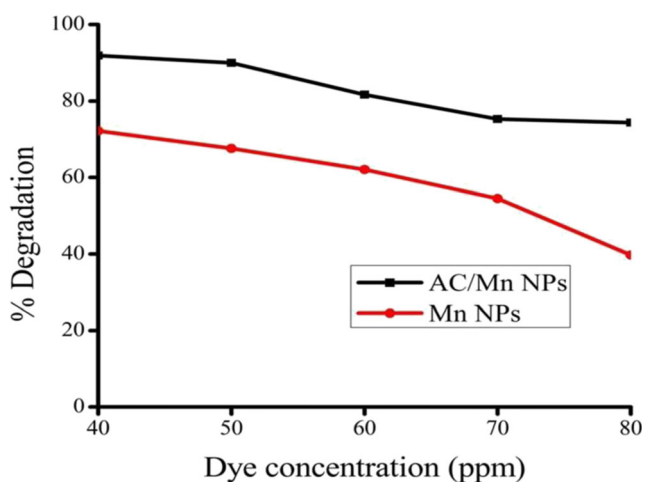


Fig. 16 Degradation rate of CR dye at various initial dye concentration photodegraded by MnO₂/AC composite and Mn NPs

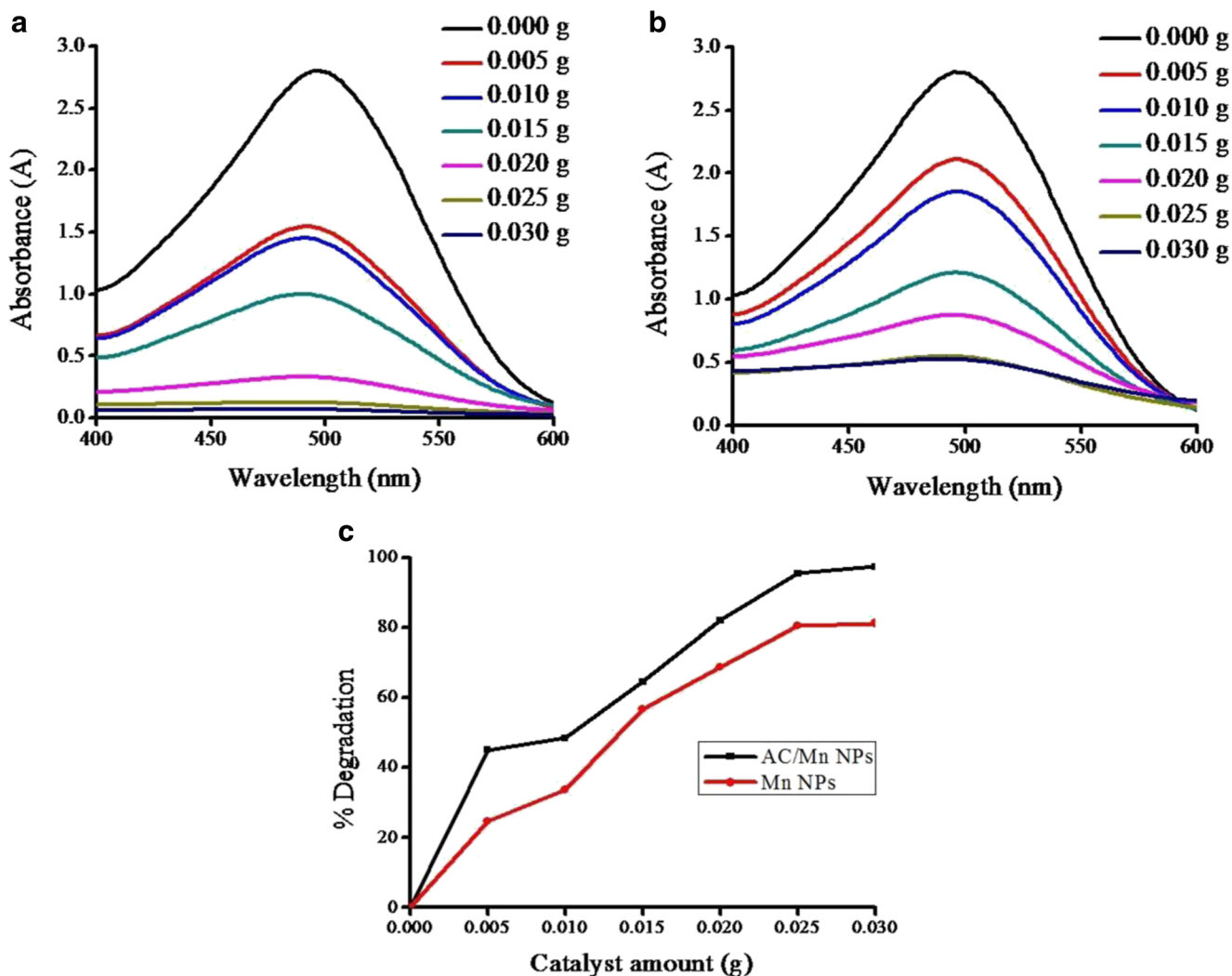


Fig. 15 UV-Visible spectra of CR photodegraded by different amount of **a** MnO₂/AC composite, **b** MnO₂ NPs, and **c** degradation comparison with different amount of MnO₂/AC and MnO₂ NPs

photodegradation efficiency of MnO₂/AC composite was higher than neat MnO₂ NPs. The 0.005 g MnO₂/AC composite and MnO₂ NPs degraded CR about 45.1% and 24.75% which increased to 97.5 and 81.28% by increasing photocatalyst amount to 0.030 g, respectively.

Effect of initial dye concentration

Industries discharge its effluents containing dye at unknown concentration, may be diluted or concentrated, so it is important to study the effect of initial concentration of dye on the photodegradation rate of dye. The effect of initial dye concentration was also evaluated by degrading dye at various initial dye concentrations (40, 50, 60, 70, and 80 ppm) under constant irradiation time (2 min) and catalyst amount (0.02 g). Figure 16 illustrates the % degradation of CR dye at various initial dye concentration as photodegraded by MnO₂/AC composite and MnO₂ NPs.

The result also revealed that as the dye concentration increased, it adversely affects the rate of CR dye degradation. The results show that at initial concentration of 40 ppm, the MnO₂/AC composite degraded 91.88% dye, which decreased gradually to 89.94, 81.67, 75.31, and 74.38% by increasing dye concentration to 50, 60, 70, and 80 ppm, respectively. Similarly, MnO₂ NPs degraded 72.21% dye at initial concentration of 40 ppm, which also decreased to 67.6, 62.07, 54.53, and 39.71% by increasing initial dye concentration to 50, 60, 70, and 80 ppm, respectively. Such decrease in the photodegradation efficiency might be possible that as initial dye concentration increases more quantity of dye get adsorbed on catalyst surface, which absorb significant amount of irradiating light rather the photocatalysts. The increase in dye concentration also reduces formation of hydroxyl radicals as the dye molecules occupy the active sites of the catalysts (Reza et al. 2017).

Conclusion

Activated carbon prepared from peanut had high surface area and highly stable support medium for Mn NP synthesis. The supported NPs are well dispersed on the surface of AC. The MnO₂/AC composite degraded about 98.53% of CR dye within 5 min while MnO₂ NPs degraded 66.57% of dye within the same irradiation time. The photocatalysts were also active under visible light and it was found that MnO₂/AC composite and MnO₂ NPs degraded 94.21 and 56.78%, respectively. Both the photocatalysts are sustainable but the Mn/AC composite is highly sustainable and can be reused several times for CR dye degradation by simple washing and heat treatment. In tap water, both photocatalysts are highly active, which might be due to the presence of various mineral ions in tap water.

References

- Akpan UG, Hameed BH (2009) Parameters affecting the photocatalytic degradation of dyes using TiO₂-based photocatalysts: a review. *J Hazard Mater* 170:520–529
- Dang TD, Le TTH, Hoang TBT, Mai TT (2015) Synthesis of nanostructured manganese oxides based materials and application for supercapacitor. *Adv Nat Sci Nanosci Nanotechnol* 6:025011
- Erdemoglu S, Aksu SK, Sayilkan F, Izgi B, Asilturk M, Sayilkan H, Frimmel F, Gucer S (2008) Photocatalytic degradation of Congo red by hydrothermally synthesized nanocrystalline TiO₂ and identification of degradation products by LC–MS. *J Hazard Mater* 155:469–476
- Feng L, Xuan Z, Zhao H, Bai Y, Guo J, Su C, Chen X (2014) MnO₂ prepared by hydrothermal method and electrochemical performance as anode for lithium-ion battery. *Nanoscale Res Lett* 9:290–297
- Ganeshan S, Ramasundari P, Elangovan A, Arivazhagan G, Vijayalakshmi R (2017) Synthesis and characterization of MnO₂ nanoparticles: study of structural and optical properties. *Int J Sci Res Phys Appl Sci* 5:5–8
- Gong K, Hu Q, Yao L, Li M, Sun D, Shao Q, Qiu B, Guo Z (2018) Ultrasonic pretreated sludge derived stable magnetic active carbon for Cr(VI) removal from wastewater. *ACS Sustain Chem Eng* 6:7283–7291
- Hamukwaya SL, Zengying Z, Ning W, Hu L, Ahmad U, Jiaoxia Z, Tingting W, Zhanhu G (2019) Enhanced photocatalytic activity of B, N-Codoped TiO₂ by a new molten nitrate process. *J Nanosci Nanotechnol* 19:839–949
- Huang J, Cao Y, Shao Q, Peng X, Guo Z (2017) Magnetic Nanocarbon adsorbents with enhanced hexavalent chromium removal: morphology dependence of Fibrillar vs particulate structures. *Ind Eng Chem Res* 56:10689–10701
- Huang J, Li Y, Cao Y, Peng F, Cao Y, Shao Q, Liu H, Guo Z (2018) Hexavalent chromium removal over magnetic carbon nanoadsorbents: synergistic effect of fluorine and nitrogen co-doping. *J Mater Chem A* 6:13062–13074
- Ioannidou O, Zabaniotou A (2007) Agricultural residues as precursors for activated carbon production—a review. *Renew Sust Energy Rev* 11:1966–2005
- Jaganyi D, Altaf M, Wekesa I (2013) Synthesis and characterization of whisker-shaped MnO₂ nanostructure at room temperature. *Appl Nanosci* 3:329–333
- Koo Y, Littlejohn G, Collins B, Shanov YYVN, Schulz M, Pai D, Sankar J (2014) Synthesis and characterization of ag-TiO₂-CNT nanoparticle composites with high photocatalytic activity under artificial light. *Composites Part B* 57:105–111
- Li Z, Wang B, Qin X, Wang Y, Liu C, Shao Q, Wang N, Zhang J, Shen C, Guo Z (2018) Superhydrophobic/Superoleophilic polycarbonate/carbon nanotubes porous monolith for selective oil adsorption from water. *ACS Sustain Chem Eng* 6:13747–13755. <https://doi.org/10.1021/acssuschemeng.8b01637>
- Lin C, Hu L, Cheng C, Sun K, Guo X, Shao Q, Li J, Wang N, Guo Z (2018) Nano-TiNb₂O₇/carbon nanotubes composite anode for enhanced lithium-ion storage. *Electrochim Acta* 260:65–72
- Liu S, Cai Y, Cai X, Li H, Zhang F, Mu Q, Liu Y, Wang Y (2013) Catalytic photodegradation of Congo red in aqueous solution by In(OH)₃ (In = Nd, Sm, Eu, Gd, Tb, and Dy) nanorods. *Appl Catal A Gen* 453:45–53
- Mamba G, Mbianda XY, Mishra AK (2015) Photocatalytic degradation of the diazo dye naphthol blue black in water using MWCNT/Gd,N,S-TiO₂ nanocomposites under simulated solar light. *J Environ Sci* 33:219–228
- Melghit K, Al-Rabaniah SS (2006) Photodegradation of Congo red under sunlight catalysed by nanorod rutile TiO₂. *J Photochem Photobiol A Chem* 184:331–334
- Mohamed A, El-Sayed R, Osman TA, Toprak MS, Muhammed M, Uheida A (2016) Composite nanofibers for highly efficient photocatalytic degradation of organic dyes from contaminated water. *Environ Res* 145:18–25
- Padikkaparambil S, Narayanan B, Yaakob Z, Viswanathan S, Tasirin S (2013) Au/TiO₂ reusable Photocatalysts for dye degradation. *Int J Photoenergy* 752605(2013):1–10
- Pan D, Ge S, Zhang X, Mai X, Li S, Guo Z (2018a) Synthesis and photoelectrocatalytic activity of In₂O₃ hollow microspheres via a bio-template route using yeast templates. *Dalton Trans* 47:708–715
- Pan D, Ge S, Zhao J, Shao Q, Guo L, Zhang X, Lin J, Xu G, Guo Z (2018b) Synthesis, characterization and photocatalytic activity of mixed-metal oxides derived from NiCoFe ternary layered double hydroxides. *Dalton Trans* 47:9765–9778
- Pouretedal HR, Kiyani M (2014) Photodegradation of 2-nitrophenol catalyzed by CoO, CoS and CoO/CoS nanoparticles. *J Iran Chem Soc* 11:271–277
- Reza KM, Kurny ASW, Gulshan F (2017) Parameters affecting the photocatalytic degradation of dyes using TiO₂: a review. *Appl Water Sci* 7:1569–1578
- Rout L, Rengasamy P, Ekka B, Kumar A, Dash P (2015) Supported bimetallic AgSn nanoparticle as an efficient Photocatalyst for degradation of methylene blue dye. *NANO* 10:1550059
- Sadiq M, Khan M, Numan M, Aman R, Hussain S, Ahmad MS, Sadiq S, Zia MA, Rashid HU, Ali R (2017) Tuning of activated carbon for solvent-free oxidation of cyclohexane. *J Chem* 2017:1–8. <https://doi.org/10.1155/2017/5732761>
- Saeed K, Khan I, Park SY (2015) TiO₂/amidoxime-modified polyacrylonitrile nanofibers and its application for the photodegradation of methyl blue in aqueous medium. *Desalin Water Treat* 54:3146–3151
- Saeed K, Khan I, Ahmad Z, Khan B (2018) Preparation, analyses and application of cobalt–manganese oxides/nylon 6,6 nanocomposites. *Polym Bull* 75:4657–4669. <https://doi.org/10.1007/s00289-018-2292-3>
- Sangami G, Dharmaraj N (2012) UV–visible spectroscopic estimation of photodegradation of rhodamine-B dye using tin(IV) oxide nanoparticles. *Spectrochim Acta A Mol Biomol Spectrosc* 97:847–852
- Shivaraju HP, Midhun G, Kumar KMA, Pallavi S, Pallavi N, Behzad S (2017) Degradation of selected industrial dyes using mg-doped TiO₂ polyscales under natural sun light as an alternative driving energy. *Appl Water Sci* 7:3937–3948

- Soltani RDC, Haghghat Z (2016) Visible light photocatalysis of a textile dye over ZnO nanostructures covered on natural diatomite. *Turk J Chem* 40:454–466
- Song B, Wang T, Sun H, Shao Q, Zhao J, Song K, Hao L, Wang L, Guo Z (2017) Two-step hydrothermally synthesized carbon nanodots/WO₃ photocatalysts with enhanced photocatalytic performance. *Dalton Trans* 46:15769–15777
- Su T, Shao Q, Qin Z, Guo Z, Wu Z (2018) Role of interfaces in two-dimensional Photocatalyst for water splitting. *ACS Catal* 8:2253–2276
- Velusamy P, Lakshmi G (2017) Enhanced photocatalytic performance of (ZnO/CeO₂)-b-CD system for the effective decolorization of rhodamine B under UV light irradiation. *Appl Water Sci* 7:4025–4036
- Wang H, Xie C, Zhang W, Cai S, Yang Z, Gui Y (2007) Comparison of dye degradation efficiency using ZnO powders with various size scales. *J Hazard Mater* 141:645–652
- Wang C, Murugadoss V, Kong J, He Z, Mai X, Shao Q, Chen Y, Guo L, Liu C, Angaiiah S, Guo Z (2018) Overview of carbon nanostructures and nanocomposites for electromagnetic wave shielding. *Carbon* 140:696–733
- Wu ZC, Zhang Y, Tao TX, Zhang L, Fong H (2010) Silver nanoparticles on amidoxime fibers for photo-catalytic degradation of organic dyes in waste water. *Appl Surf Sci* 257:1092–1097
- Wu T, Shao Q, Ge S, Bao L, Liu Q (2016) The facile preparation of novel magnetic zirconia composites with the aid of carboxymethyl chitosan and their efficient removal of dye. *RSC Adv* 6:58020–58027
- Yang Z, Hao X, Chen S, Ma Z, Wang W, Wang C, Yue L, Sun H, Shao Q, Murugadoss V, Guo Z (2019) Long-term antibacterial stable reduced graphene oxide nanocomposites loaded with cuprous oxide nanoparticles. *J Colloid Interface Sci* 533:13–23
- Zada N, Khan I, Saeed K (2017) Synthesis of multiwalled carbon nanotubes supported manganese and cobalt zinc oxides nanoparticles for the photodegradation of malachite green. *Sep Sci Technol* 52:1477–1485
- Zhang D, Zeng F (2010) Structural, photochemical and photocatalytic properties of zirconium oxide doped TiO₂ nanocrystallites. *Appl Surf Sci* 257:867–871
- Zhang L, Qin M, Yu W, Zhang Q, Xie H, Sun Z, Shao Q, Guo X, Hao L, Zheng Y, Guo Z (2017a) Heterostructured TiO₂/WO₃ nanocomposites for photocatalytic degradation of toluene under visible light. *J Electrochem Soc* 164:H1086–H1090
- Zhang L, Yu W, Han C, Guo J, Zhang Q, Xie H, Shao Q, Sun Z, Guo Z (2017b) Large scaled synthesis of Heterostructured electrospun TiO₂/SnO₂ nanofibers with an enhanced photocatalytic activity. *J Electrochem Soc* 164:H651–H656
- Zhang Y, Qian L, Zhao W, Li X, Huang X, Mai X, Wang Z, Shao Q, Yan X, Guo Z (2018) Highly efficient Fe-N-C nanoparticles modified porous graphene composites for oxygen reduction reaction. *J Electrochem Soc* 165:H510–H516
- Zhao J, Ge S, Liu L, Shao Q, Mai X, Zhao CX, Hao L, Wu T, Yu Z, Guo Z (2018a) Microwave Solvothermal fabrication of zirconia hollow microspheres with different morphologies using pollen templates and their dye adsorption removal. *Ind Eng Chem Res* 57:231–241
- Zhao J, Ge S, Pan D, Shao Q, Lin J, Wang Z, Hu Z, Wu T, Guo Z (2018b) Solvothermal synthesis, characterization and photocatalytic property of zirconium dioxide doped titanium dioxide spinous hollow microspheres with sunflower pollen as bio-templates. *J Colloid Interface Sci* 529:111–121
- Zhao B, Shao Q, Hao L, Zhang L, Liu Z, Zhang B, Ge S, Guo Z (2018c) Yeast-template synthesized Fe-doped cerium oxide hollow microspheres for visible photodegradation of acid orange 7. *J Colloid Interface Sci* 511:39–47
- Zhua H, Jiang R, Xiao L, Chang Y, Guan Y, Li X, Zeng G (2009) Photocatalytic decolorization and degradation of Congo red on innovative crosslinked chitosan/nano-CdS composite catalyst under visible light irradiation. *J Hazard Mater* 169:933–940